

Unified Source-Free Domain Adaptation

Song Tang, Wenxin Su, Mao Ye✉, Jianwei Zhang and Xiatian Zhu✉

Abstract—In the pursuit of transferring a source model to a target domain without access to the source training data, Source-Free Domain Adaptation (SFDA) has been extensively explored across various scenarios, including closed-set, open-set, partial-set, and generalized settings. Existing methods, focusing on specific scenarios, not only address only a subset of challenges but also necessitate prior knowledge of the target domain, significantly limiting their practical utility and deployability. In light of these considerations, we introduce a more practical yet challenging problem, termed *unified SFDA*, which comprehensively incorporates all specific scenarios in a unified manner. To tackle this unified SFDA problem, we propose a novel approach called *Latent Causal Factors Discovery* (LCFD). In contrast to previous alternatives that emphasize learning the statistical description of reality, we formulate LCFD from a causality perspective. The objective is to uncover the causal relationships between latent variables and model decisions, enhancing the reliability and robustness of the learned model against domain shifts. To integrate extensive world knowledge, we leverage a pre-trained vision-language model such as CLIP. This aids in the formation and discovery of latent causal factors in the absence of supervision in the variation of distribution and semantics, coupled with a newly designed information bottleneck with theoretical guarantees. Extensive experiments demonstrate that LCFD can achieve new state-of-the-art results in distinct SFDA settings, as well as source-free out-of-distribution generalization. Our code and data are available at <https://github.com/tntek/source-free-domain-adaptation>.

Index Terms—Unified domain adaptation, source-free, statistical association, latent causal factors, information bottleneck.

1 INTRODUCTION

Due to escalating demands for privacy and information protection in public security and commercial competition, well-annotated training data are recognized as crucial for varying purposes, requiring stringent access control. However, in practical scenarios, the use of a source model (pre-trained on the source domain) without access to the actual source data, referred to as Source-Free Domain Adaptation (SFDA) [1], has become more feasible. This approach involves the challenges posed by strict data access controls and emphasizes the adaptation of a pre-trained model to new domains without relying on the availability of the original source data.

SFDA has been explored across various scenarios, as summarized in Table 1. The most constrained scenario, termed *closed-set*, assumes identical categories of interest in both the source and target domains, focusing on addressing covariate shift, such as domain-specific appearance distributions [2]. *Generalized SFDA* extends this by requiring the adapted model to perform well in both the source and target domains without forgetting the source domain [3]. Moving beyond the vanilla category identity constraint, *open-set* SFDA [4] considers the target domain with additional

TABLE 1: Summary of different SFDA settings. C_s/C_t : The category set of the source/target domain.

Setting	Covariate shift	Semantic shift	Anti-forgetting	Category
Closed-set	✓	✗	✗	$C_s = C_t$
Generalized	✓	✗	✓	$C_s = C_t$
Open-set	✓	✓	✗	$C_s \subset C_t$
Partial-set	✓	✓	✗	$C_s \supset C_t$
Unified (Ours)	✓	✓	✓	Any

categories, while *partial-set* SFDA [5] takes the opposite direction. Both scenarios require handling the additional challenge of semantic shift.

Typically, prevalent SFDA methods tend to concentrate on particular scenarios, tackling only a subset of challenges. For instance, SFDA-DE [6] focuses on closed-set scenarios, SF-PGL [7] on open-set scenarios, PSAT [8] on generalized settings, and CRS [9] on partial-set scenarios. Nevertheless, this approach significantly restricts their practical utility and deployability, given that we often possess limited prior knowledge about the target domain and minimal control or selection over its conditions.

To address the aforementioned limitation, this study introduces a more realistic and challenging problem, referred to as *Unified Source-Free Domain Adaptation (Unified SFDA)*, with the goal of comprehensively addressing all the specific scenarios mentioned earlier in a unified manner. To achieve this, we propose a novel approach called *Latent Causal Factors Discovery (LCFD)*, going beyond the conventional statistical association learning of related variables by exploring the underlying causal relationships [10]. The discovered causal mechanism is expected to be more reliable under varying distributions and semantic contexts, providing a unified solution for distinct SFDA scenarios.

In the absence of label supervision for both distributional

✉ Corresponding authors: Mao Ye, Xiatian Zhu.

Song Tang is with the Institute of Machine Intelligence, University of Shanghai for Science and Technology, Shanghai, China; the TAMS Group, Department of Informatics, Universität Hamburg, Hamburg, Germany.

Wenxin Su is with the Institute of Machine Intelligence, University of Shanghai for Science and Technology, Shanghai, China.

Mao Ye is with the School of Computer Science and Engineering, University of Electronic Science and Technology of China, Chengdu, China.

Jianwei Zhang is with the TAMS Group, Department of Informatics, Universität Hamburg, Hamburg, Germany.

Xiatian Zhu is with the Surrey Institute for People-Centred Artificial Intelligence, and Centre for Vision, Speech and Signal Processing, University of Surrey, Guildford, UK.

Manuscript received April 19, 20**; revised August 26, 20**.

and semantic variations, our LCFD is specifically formulated using a structural causal model in the logits space. The latent causal factors are disentangled into two complementary parts: (i) *external causal factors* and (ii) *internal causal factors*, consider that the information of both domain is not necessarily complete. For the former, we leverage a pre-trained large Vision-Language (ViL) model with rich knowledge such as CLIP [11], which has been exposed to a vast amount of multimodality information sources. The latter is identified under the guidance of discovered external causal factors. The discovery of external and internal causal factors is alternated by designing a self-supervised information bottleneck with theoretical guarantees.

Our **contributions** are summarized as follows:

- (i) For the first time, we introduce a unified SFDA problem that comprehensively incorporates various specific scenarios. This design eliminates the need for prior knowledge about the target domain before model deployment, enhancing practical usability and applicability in real-world scenarios.
- (ii) We introduce a novel approach for unified SFDA, termed LCFD. Instead of learning the statistical description of the problem reality as conventional methods do, our LCFD is formulated under the causality perspective. It aims to reveal the underlying causal relationships between latent variables and model decisions, providing favorable robustness against both distributional and semantic shifts.
- (iii) Extensive experiments demonstrate that LCFD consistently achieves new state-of-the-art results on varying SFDA scenarios as well as source-free out-of-distribution generalization.

2 RELATED WORK

2.1 Source-Free Domain Adaptation

Most of the prior SFDA methods consider the closed-set setting where the source and target domains share the same classes and the focus is cross-domain distribution alignment. Existing methods exist in two categories. The first converts SFDA to Unsupervised Domain Adaptation (UDA) by constructing a pseudo-source domain [12], exploiting source prototype-guided data generation [13] or splitting source-like subset from target data [14]. The second follows the paradigm of self-supervised learning [15], [16], introducing self-guidance. Besides widely used pseudo-labels [15], [17], geometry information [18], [19], [20], constructive data [9] and historical data [8] have also been exploited.

Recently, more practical settings have been studied. For example, the generalized setting shifts aims to mitigate forgetting the source domain [3]. A representative approach is combining continue learning techniques with cross-domain adaptation, e.g., the domain attention-based gradient regulation [3] and source guidance constructed by historical information refining [8]. There exist works considering open-set [7] and partial-set [21] settings. For instance, to control the open-set risk, a progressive balanced pseudo-labeling strategy [7] and closed-set class prototypes are proposed [22]. Estimating the target data distribution helps with negative transfer reduction from the partial classes shift [23].

Alternatively, some works were proposed to enhance the discriminating ability for out-of-distribution classes [24]. There are two main strategies: Expanding inter-class distance to prevent semantic confusion [15], [25], and introducing external semantics, e.g., CLIP, to match out-of-distribution [26].

Existing works as above focus on a specific SFDA setting, limiting their usability and generality substantially in practice. To address this limitation, we introduce a unified SFDA setting that incorporates all the pre-existing scenarios. With this new setup, we aim to foster more advanced SFDA methods that could generalize to a variety of problem settings without the need for designing and maintaining an array of distinct algorithms.

2.2 Causality methods in transfer learning

Causality methods aim for a robust function relation between random variables, which is insensitive to the extra variation/disturbing [27]. This property leads to recent popularity of this new paradigm in transfer learning, e.g., UDA [28], domain generalization (DG) [29] and out of distribution (OOD) [30]. These attempts aim to reduce non-causal factors by introducing artificial intervention. For example, the probability distribution change (used to represent the domain shift) and semantic consistency constraint are jointly employed to implement this intervention. As source labels are available to ensure consistency, these methods put the highlight on constructing the distribution change, following in two lines. One explicitly generates augmented data to disturb the distribution, e.g., the non-linear augmentation and spatially-variable blending augmentation [31], inverse Fourier transformation augmentation [32], and generative models-based cross-domain image style transformation [33], [34]. The other implicitly modifies the distribution by exploiting cross-domain data. For example, MatchDG [35] developed cross-domain contrastive learning where input's positive sample was randomly selected from samples with the same class. COR [30] adopted the variational inference encoder to infer unobserved causal factors from historical data, taking the time domain as a natural distribution change.

Compared with the existing works, the following three features distinguish LCFD from them. (i) LCFD does not rely on real labels that are indispensable for previous works. (ii) LCFD discovers the causal factors instead of indirectly removing the non-causal ones. (iii) LCFD builds the structural causal model at the logits level whilst previous methods construct on raw data.

3 METHODOLOGY

3.1 Unified SFDA problem

SFDA aims to transfer a model pre-trained on the source domain to a different but related target domain without labelling. Formally, let $\mathcal{X}_s = \{\mathbf{x}_i^s\}_{i=1}^{n_s}$ and $\mathcal{Y}_s = \{y_i^s\}_{i=1}^{n_s}$ be the source samples and their truth labels. Similarly, the unlabeled samples and the truth target labels are $\mathcal{X} = \{\mathbf{x}_i\}_{i=1}^n$ and $\mathcal{Y} = \{y_i\}_{i=1}^n$, respectively. The unified SFDA task is to learn a target model $f_{\theta_t} : \mathcal{X} \rightarrow \mathcal{Y}$ without any prior knowledge of the target domain not the relationships between the source and target domains (see Tab. 1), given (i) the source model f_{θ_s} pre-trained over \mathcal{X}_s , \mathcal{Y}_s , and (ii) the unlabeled target data \mathcal{X} .

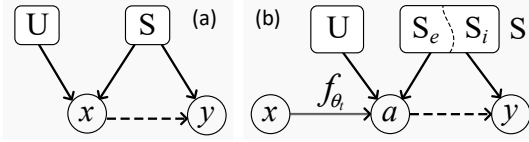


Fig. 1: Comparison of Structural Causal Models (SCM). (a) SCM for transfer learning with source domain, where S and U represent causal and non-causal factors. Domain shift is generally caused by U , which, together with the generalizable information S , e.g., the shape/structure of a dog (see Fig. 2), form the observation x . (b) Our proposed SCM for SFDA in a latent space (e.g., the logit a) where the causal factors S are decomposed into the external S_e and internal S_i components.

3.2 Causality in transfer learning with source domain

In transfer learning with source domain available, such as DG, and UDA, the causality relation hidden in the statistical dependence (between raw image x and available label y) can be summarized to a Structural Causal Model (SCM). As depicted in Fig. 1(a), x is generated jointly by non-causal factors U and causal factors S , while label y is determined by S alone. Here, non-causal factors collectively represent the latent variables that generate the category-independent appearance of images, e.g., different domain styles and spurious dependence (Fig. 2); The causal factors present the ones determining the classification, e.g., the object shape.

In a causal view, solving the transfer learning involves eliminating the domain shift by building a robust classification function, i.e., $P(y|S)$. With SCM, we need to disconnect U to x . So existing works impose intervention upon x , according to the intervention theory [10]. Formally, this scheme can be formulated as

$$P(y|S) = P(y|do(x), S), \quad (1)$$

where $do(\cdot)$ means the do-operation of imposing intervention upon variables.

In summary, the key idea is when we change the probability distribution of non-causal factors (intervention) whilst keep the category (prediction consistency), the causality can be extracted. Often, domain related data augmentation is adopted as intervention, whilst the source labels ensure prediction consistency. However both conditions are unavailable in SFDA, making it inapplicable.

3.3 Latent Causality in Unified SFDA

To address the challenges outlined earlier, we propose an approach named *Latent Causal Factors Discovery* (LCFD), taking into account the following considerations. Instead of extracting causality in the raw input space x , we shift our focus to the logit space \mathcal{A} : $a = f_{\theta_t}(x) \in \mathcal{A}$. The choice of this space for causality analysis is crucial for two main reasons. First, at the presence of domain distribution gap during adaptation, using the logits essentially imposes a probability distribution perturbation, which could be considered as a special sort of intervention. This post-intervention property facilitates the extraction of causal factors [10], [30], [35]. Second, integration of additional information sources becomes

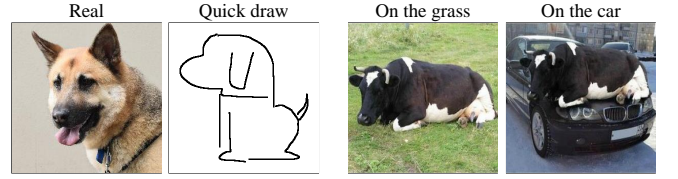


Fig. 2: Illustration of domain shift. (a) **Different appearance styles** of dog; (b) **Spurious dependence of background**: Cow in grass ground vs. on a car.

simpler in this semantic space, without being constrained by distinct model architectures.

An overview of our LCFD is depicted in Fig. 1(b). It models non-causal U and causal S factors in a latent space \mathcal{A} . Uniquely, the causal part is further decomposed into internal S_i and external S_e components, consider that the information of source and target domain is not necessarily comprehensive. In contrast to conventional intervention driven learning, we focus on discovering S from the intertwined S and U as

$$P(y|S) = P(y|dis(S|\{U, S\})), \quad S = \{S_i, S_e\}. \quad (2)$$

To make this process computationally tractable, we consider **Principle 1. Independent Causal Mechanisms Principle [36]**:

The conditional distribution of each variable given its causes (i.e., its mechanism) does not inform or influence the other mechanisms.

This principle means S_i and S_e are independent in our context. So we can simplify our above formula as:

$$P(y|S) = P(y|dis(S_e|\{U, S_e\})) \cdot P(y|dis(S_i|\{U, S_i\})). \quad (3)$$

3.4 LCFD Design

We present a concrete design for realizing the LCFD as formulated above. An overview is depicted in Fig. 3. By Eq. (3), we implement the causality discovery in two parts: phase-1 for S_e and phase-2 for S_i , as detailed below.

3.4.1 External Causality Discovery

To obtain external causality for a target task, we explore the potential of recent large multimodal ViL models such as CLIP [11]. This is because they have experienced a vast amount of knowledge in pretraining, and exhibited general ability in many different perception tasks.

Specifically, we accomplish this idea by encoding S_e into the prompt context v_e of a ViL model g_{θ} efficiently. That is, our learning target is v_e , which is the explicit expression of S_e . We start by formulating the S_e discovery as maximizing the correlation between a random variable representing S_e and the prediction of the target model. Then, the original formulation is converted to a self-supervised information bottleneck problem with theoretical guarantee, followed by the deep learning instantiation.

With the target samples \mathcal{X} and learnable v_e , we obtain the prediction of g_{θ} as $\hat{P} = \{\hat{p}_i\}_{i=1}^n$. Meanwhile, we obtain the logits of target model f_{θ_t} for the same data as $\mathcal{A} = \{a_i\}_{i=1}^n$. We introduce three random variables, V , Y , and Z , following the probability distributions of v_e , \hat{P} and \mathcal{A} , respectively.

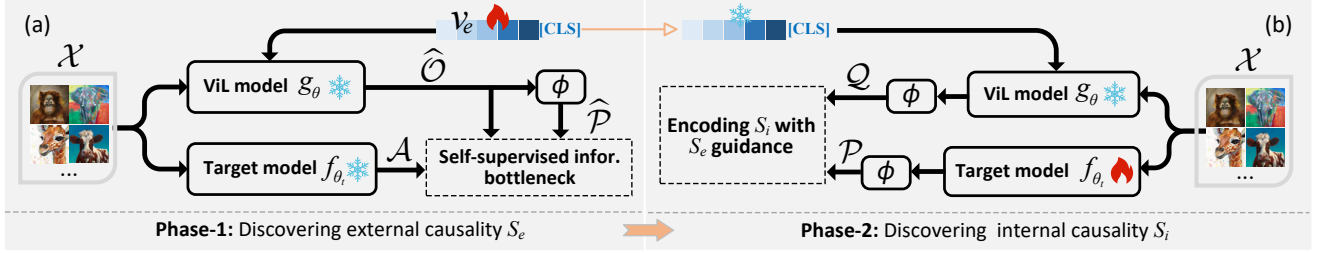


Fig. 3: Overview of our proposed LCFD framework: (a) Phase-1: Discovering the external causal factors S_e in form of prompt context v_e from a frozen ViL model using our self-supervised information bottleneck algorithm; (b) Phase-2: Discovering the internal causal factors S_i where the updated prompt context v_e is used to predict pseudo-labels as the prior information.

In LCFD, we further write $Z = \{Z_e, Z_i\}$ where the latent random variables Z_e and Z_i represent the external S_e and the internal S_i causal factors, respectively.

In information-theoretic view, for causality relationships we have to ensure the correlation between Z_e and V . This could be considered an approximation with computational ease. Formally, discovering S_e needs maximizing the following mutual information:

$$\max_{v_e} I(Z_e, V), \quad (4)$$

where function $I(\cdot, \cdot)$ computes mutual information of two random variables.

Consider that prompt V is specific to the ViL model g_θ , we further transform the above formula as

$$\max_{v_e} I(Z_e, Y) = \phi(g_\theta(V)), \quad (5)$$

where $\phi(\cdot)$ is softmax function; so that the two variables under correlation maximization reside in similarly semantic spaces. Theoretically, we prove that this transformed is a low bound of the original, thus valid in terms of optimization.

First, we have the following **Lemma 1** (see the proof in Appendix).

Lemma 1. Given random variables Z_1, X_1 and Y_1 where X_1, Y_1 satisfy a mapping $f_1 : X_1 \mapsto Y_1$. When f_1 is compressed, i.e., the output's dimension is smaller than the input's,

$$I(Z_1, X_1) \geq I(Z_1, Y_1). \quad (6)$$

The ViL model g_θ is indeed compressing, as it maps a high-dimensional image to a low-dimensional category vector. Letting $Z_1 = Z_e, X_1 = X, Y_1 = Y$ and $f_1 = \phi(g_\theta(\cdot))$, we have $I(Z_e, V) \geq I(Z_e, Y)$ according to **Lemma 1**.

Self-supervised information bottleneck. In Eq. (5), Z_e is hidden part of the observable logits along with non-causal and internal causal factors. To facilitate this learning process of Z_e , we derive a self-supervised information bottleneck algorithm without prior assumption on the distribution [37]. In general, information bottleneck conducts min-max optimization to squeeze out the essentials w.r.t. a task. We introduce a random variable Z' (i.e., the bottleneck) for the ViL's logits $\hat{O} = \{\hat{o}_i\}_{i=1}^n$ between V and Y , thereby forming a bottleneck style expression as:

$$\min_{v_e} I(Z, Z') - I(Z', Y), \quad (7)$$

where Z is the logit variable of target model f_{θ_t} which is observed. Note, we do not include the item $I(Z', Y)$ in minimization due to lacking of supervision signal like ground-truth labels as used in conventional information bottleneck [38], i.e., a self-supervised formulation. However, we theoretically prove that Eq. (7) is an upper bound as below thus optimally valid.

Theorem 1. Suppose that there are five random variables Z, V, Z', Y and Y' . Among them, Z represents the target domain knowledge; V, Z' and Y express the input instances, an intermediate features of the ViL model and predictions, respectively; Y' depicts a pseudo-label that has a functional relationship f_w (w is learnable parameters) with Z' . When f_w is reversible and uncompressed, we have this upper bound

$$\begin{aligned} & \min_{v_e} I(Z, Z') - I(Z', Y) \\ & \leq \underbrace{\min_{v_e, w} I(Z, Z')}_{T_1} - \underbrace{I(Y', Y), Y' = f_w(Z')}_{T_2}. \end{aligned} \quad (8)$$

The proof is given in Appendix ?? **Theorem 1** suggests that the desired latent factors refinement is conditionally equivalent to a self-supervised information bottleneck, when pseudo-label Y' is generated from the intermediate ViL feature Z' without information loss.

We realize the proposed information bottleneck using variational information maximization [39]. The key is to construct the function f_w with three properties: (i) The output is a probability distribution, e.g., including a softmax operation ϕ . (ii) No information loss, e.g., no zero weights in w for weighting based functions. (iii) The weighting parameters w are constrained to be relevant to $I(Z', Z)$. The instantiation of T_1 and T_2 are elaborated below.

As exactly computing mutual information of two vector variables is intractable, we maximize the variational lower bound for the term T_1 (see the proof in [40]):

$$\begin{aligned} I(Z, Z') &= \mathbb{E}_{Z, Z'} \left[\log \frac{q(Z'|Z)}{p(Z')} \right] + \text{KL}(q(Z'|Z) \| p(Z'|Z)) \\ &\geq H(Z') + \mathbb{E}_{Z, Z'} (\log q(Z'|Z)), \end{aligned} \quad (9)$$

where $q(Z'|Z)$ is variational distribution approximating the real distribution $p(Z'|Z)$, $\text{KL}(\cdot, \cdot)$ is KL-divergence function, and $H(Z')$ is a constant. In practice, we model $q(Z'|Z)$ as a Gaussian distribution $\mathcal{N}(Z, \Sigma_Z)$ with mean Z and diagonal

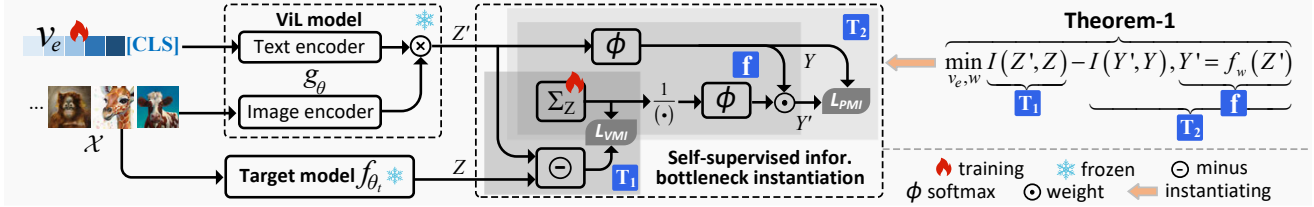


Fig. 4: Realising our self-supervised information bottleneck w.r.t. **Theorem 1**. The item T_1 is estimated by variational information maximization with Gaussian distribution assumption $\mathcal{N}(Z, \Sigma_Z)$. The item T_2 is computed by mutual information definition where the function f_w integrates the min-max optimization, using covariance matrix Σ_Z from T_1 as the weighting parameters w .

covariance matrix Σ_Z . Then, the loss for minimizing T_1 can be formulated (see T_1 in Fig. 4):

$$\begin{aligned} \mathcal{L}_{\text{VMI}}(\mathcal{X}; \mathbf{v}_e, \Sigma_Z) &= -\mathbb{E}_{Z, Z'} \left(\|Z' - Z\|_{\Sigma_Z^{-1}}^2 + \log |\Sigma_Z| \right) \\ &= -\frac{1}{n} \sum_{i=1}^n (\hat{\mathbf{o}}_i - \mathbf{a}_i)^T \Sigma_Z^{-1} (\hat{\mathbf{o}}_i - \mathbf{a}_i) + \log |\Sigma_Z|. \end{aligned} \quad (10)$$

Considering that the ViL's prediction Y and the pseudo-label Y' are probability distributions, we compute the second term T_2 by the original mutual information [41]: $I(Z, Z') = p(Z, Z')/[p(Z)p(Z')]$. The corresponding loss function is

$$\begin{aligned} \mathcal{L}_{\text{PMI}}(\mathcal{X}; \mathbf{v}_e, \Sigma_Z) &= \frac{1}{n} \sum_{i=1}^n I(\hat{\mathbf{p}}_i, \mathbf{p}'_i), \\ \hat{\mathbf{p}}_i &= \phi(\hat{\mathbf{o}}_i), \quad \mathbf{p}'_i = f_w(\hat{\mathbf{o}}_i) \end{aligned} \quad (11)$$

where f_w is a weighting-based function we construct as follows.

From Eq. (10), $I(Z', Z)$ is a Mean-Square Error (MSE) weighted by Σ_Z . That means Σ_Z detects dimension importance duration minimization, with high-weight dimensions to be suppressed, thus corresponding to the non-causal factors U in our formulation. Thus, taking $1/\Sigma_Z$ as the weighting parameters of f_w shifts the focus of predicting to the causal component S_e (see \mathbf{f} in Fig. 4), formally,

$$\mathbf{p}'_i = f_{[w=\Sigma_Z^i]}(\hat{\mathbf{o}}_i) = \phi\left(\frac{1}{\Sigma_Z^i}\right) \odot \phi(\hat{\mathbf{o}}_i). \quad (12)$$

Combining Eq. (10), (11) and (12) together, our self-supervised objective for external causality discovery is formed as

$$\begin{aligned} \min_{\mathbf{v}_e, \Sigma_Z} \mathcal{L}_{\text{EC}}(\mathcal{X}; \mathbf{v}_e, \Sigma_Z) \\ = \mathcal{L}_{\text{PMI}}(\mathcal{X}; \mathbf{v}_e, \Sigma_Z) - \alpha \mathcal{L}_{\text{VMI}}(\mathcal{X}; \mathbf{v}_e, \Sigma_Z). \end{aligned} \quad (13)$$

Remark. Our design differs from existing information bottleneck in two aspects: While previous information extraction [42] is confined to a single model, ours is of cross-model. Our formulation is self-supervised, in contrast to previous supervised designs.

3.4.2 Internal Causality Discovery

In phase-2, we subsequently discover the internal causal factors S_i by updating the target model. That is, we encode S_i into the target model as it is latent in nature. This is achieved using the pseudo-labels predicted by the ViL model and prompt context in a self-supervised learning manner.

Algorithm 1 Training LCFD

Input: Unlabelled target data \mathcal{X} , pre-trained source model f_{θ_s} , a frozen ViL model g_{θ} , max training iteration number M , prompt context \mathbf{v}_e .

- 1: Initialize the target model f_{θ_t} by f_{θ_s}
- 2: Initialize \mathbf{v}_e with a fixed template
- 3: **for** iter $k = 1$ to M **do**
- 4: Sample a mini-batch \mathcal{X}_b from \mathcal{X} .
- 5: Discover external causal factors S_e : update (\mathbf{v}_e, Σ_Z) by optimizing $\mathcal{L}_{\text{EC}}(\mathcal{X}_b; \mathbf{v}_e, \Sigma_Z)$, fixing \mathcal{L}_{IC} .
- 6: Convert updated \mathbf{v}_e to target pseudo-labels for this batch \mathcal{X}_b , i.e., obtain $\mathcal{Q}_b = \phi(g_{\theta}(\mathcal{X}_b, \mathbf{v}_e))$.
- 7: Discover internal causal factors S_i : update f_{θ_t} by optimizing \mathcal{L}_{IC} , fixing \mathcal{L}_{EC} .
- 8: **end for**
- 9: **return:** The adapted model f_{θ_t} .

Formally, denote $\mathcal{Q} = \phi(g_{\theta}(\mathcal{X}, \mathbf{v}_e))$ the pseudo-labels of the target data \mathcal{X} generated by the ViL model g_{θ} , using \mathbf{v}_e updated in phase-1, and $\mathcal{P} = \phi(f_{\theta_t}(\mathcal{X}))$ the predictions of \mathcal{X} by the target model f_{θ_t} . We design the objective function for discovering S_i as

$$\mathcal{L}_{\text{IC}} = \min_{\theta_t} H(\mathcal{P}) + \tau \underbrace{\sum_{c=1}^C \text{KL}\left(\varrho_c \parallel \frac{1}{C}\right)}_{\mathcal{L}_{\text{UN}}} + \sigma \underbrace{\mathcal{L}_{\text{SCE}}(\mathcal{P}, \mathcal{Q}; \theta_t)}_{\mathcal{L}_{\text{PL}}} \quad (14)$$

where $H(\mathcal{P}) = -\sum_{i=1}^n \mathbf{p}_i \log \mathbf{p}_i$ estimates the information entropy, $\frac{1}{C}$ stands for the uniform distribution over C categories, $\varrho_c = \frac{1}{n} \sum_{i=1}^n p_{i,c}$ is empirical label distribution, $p_{i,c}$ is the probability of \mathbf{x}_i in the c -th category, \mathcal{L}_{SCE} is the softmax-cross-entropy loss, and τ, σ are trade-off parameters. The first term \mathcal{L}_{UN} is a regularization for encouraging prediction confidence and avoiding solution collapse [43]. Aligning with the pseudo labels estimated using the prompt context, the second item \mathcal{L}_{PL} essentially integrates the external causal factors S_e while learning S_i .

3.5 Model Training

We train LCFD in an alternating manner. In each iteration, we first optimize prompt context \mathbf{v}_e with \mathcal{L}_{EC} whilst the target model is frozen (i.e., phase-1), followed by training the target model by \mathcal{L}_{IC} (i.e., phase-2) while the prompt context is frozen. The ViL model is always frozen throughout. More details for training is presented in Alg. 1.

TABLE 2: Closed-set SFDA results (%) on **Office-Home** and **VisDA**. SF and M means source-free and multimodal, respectively.

Method	Venue	SF	M	Office-Home												VisDA	
				Ar→Cl	Ar→Pr	Ar→Rw	Cl→Ar	Cl→Pr	Cl→Rw	Pr→Ar	Pr→Cl	Pr→Rw	Rw→Ar	Rw→Cl	Rw→Pr	Avg.	
Source	—	—	—	43.7	67.0	73.9	49.9	60.1	62.5	51.7	40.9	72.6	64.2	46.3	78.1	59.2	49.2
CLIP-RN	ICML21	—	✓	51.9	81.5	82.5	72.5	81.5	82.5	72.5	51.9	82.5	72.5	51.9	81.5	72.1	83.7
CLIP-B32	ICML21	—	✓	59.8	84.3	85.5	74.6	84.3	85.5	74.6	59.8	85.5	74.6	59.8	84.3	76.1	82.9
DAPL-RN	TNNLS23	✗	✓	54.1	84.3	84.8	74.4	83.7	85.0	74.5	54.6	84.8	75.2	54.7	83.8	74.5	86.9
PADCLIP-RN	ICCV23	✗	✓	57.5	84.0	83.8	77.8	85.5	84.7	76.3	59.2	85.4	78.1	60.2	86.7	76.6	88.5
ADCLIP-RN	ICCV23W	✗	✓	55.4	85.2	85.6	76.1	85.8	86.2	76.7	56.1	85.4	76.8	56.1	85.5	75.9	87.7
SHOT	ICML20	✓	✗	55.0	78.7	81.3	69.1	78.9	79.1	68.2	53.6	81.6	73.5	59.4	83.5	71.8	82.9
GKD	IROS21	✓	✗	56.5	78.3	82.2	69.2	80.4	78.7	67.4	55.4	82.6	74.3	60.3	84.2	72.5	83.0
NRC	NIPS21	✓	✗	57.2	79.3	81.3	68.9	80.6	80.2	66.6	57.3	82.0	71.0	57.9	84.9	72.3	85.9
AaD	NIPS22	✓	✗	59.3	79.3	82.1	68.9	79.8	79.5	67.2	57.4	83.1	72.1	58.5	85.4	72.7	88.0
AdaCon	CVPR22	✓	✗	47.2	75.1	75.5	60.7	73.3	73.2	60.2	45.2	76.6	65.6	48.3	79.1	65.0	86.8
CoWA	ICML22	✓	✗	57.3	79.3	81.0	69.3	77.9	79.6	68.1	56.4	82.6	72.9	61.3	83.7	72.4	86.9
PLUE	CVPR23	✓	✗	49.1	73.5	78.2	62.9	73.5	74.5	62.2	48.3	78.6	68.6	51.8	81.5	66.9	88.3
TPDS	IJCV23	✓	✗	59.3	80.3	82.1	70.6	79.4	80.9	69.8	56.8	82.1	74.5	61.2	85.3	73.5	87.6
LCFD-C-RN	—	—	✓	60.1	85.6	86.2	77.2	86.0	86.3	76.6	61.0	86.5	77.5	61.4	86.2	77.6	89.3
LCFD-C-B32	—	—	✓	72.3	89.8	89.9	81.1	90.3	89.5	80.1	71.5	89.8	81.8	72.7	90.4	83.3	89.3

TABLE 3: Closed-set SFDA results (%) on **DomainNet-126**. SF and M means source-free and multimodal, respectively.

Method	Venue	SF	M	C→P	C→R	C→S	P→C	P→R	P→S	R→C	R→P	R→S	S→C	S→P	S→R	Avg.
Source	—	—	—	44.6	59.8	47.5	53.3	75.3	46.2	55.3	62.7	46.4	55.1	50.7	59.5	54.7
CLIP-RN	ICML21	—	✓	70.2	87.1	65.4	67.9	87.1	65.4	67.9	70.2	65.4	67.9	70.2	87.1	72.7
CLIP-B32	ICML21	—	✓	73.5	85.7	71.2	74.7	85.7	71.2	74.7	73.5	71.2	74.7	73.5	85.7	76.3
DAPL-RN	TNNLS23	✗	✓	72.4	87.6	65.9	72.7	87.6	65.6	73.2	72.4	66.2	73.8	72.9	87.8	74.8
ADCLIP-RN	ICCV23W	✗	✓	71.7	88.1	66.0	73.2	86.9	65.2	73.6	73.0	68.4	72.3	74.2	89.3	75.2
SHOT	ICML20	✓	✗	63.5	78.2	59.5	67.9	81.3	61.7	67.7	67.6	57.8	70.2	64.0	78.0	68.1
GKD	IROS21	✓	✗	61.4	77.4	60.3	69.6	81.4	63.2	68.3	68.4	59.5	71.5	65.2	77.6	68.7
NRC	NIPS21	✓	✗	62.6	77.1	58.3	62.9	81.3	60.7	64.7	69.4	58.7	69.4	65.8	78.7	67.5
AdaCon	CVPR22	✓	✗	60.8	74.8	55.9	62.2	78.3	58.2	63.1	68.1	55.6	67.1	66.0	75.4	65.4
CoWA	ICML22	✓	✗	64.6	80.6	60.6	66.2	79.8	60.8	69.0	67.2	60.0	69.0	65.8	79.9	68.6
PLUE	CVPR23	✓	✗	59.8	74.0	56.0	61.6	78.5	57.9	61.6	65.9	53.8	67.5	64.3	76.0	64.7
TPDS	IJCV23	✓	✗	62.9	77.1	59.8	65.6	79.0	61.5	66.4	67.0	58.2	68.6	64.3	75.3	67.1
LCFD-C-RN	—	—	✓	75.4	88.2	72.0	75.8	88.3	72.1	76.1	75.6	71.2	77.6	75.9	88.2	78.0
LCFD-C-B32	—	—	✓	77.2	88.0	75.2	78.8	88.2	75.8	79.1	77.8	74.9	79.9	77.4	88.0	80.0

4 EXPERIMENTS

4.1 Implementation Details

Source models. Following [44], for source-free out-of-distribution generalization (SF-OODG) we adopt the Pytorch built-in ResNet50 model (pre-trained on ImageNet) as the source model, taking ImageNet variations as evaluation datasets. For all the other settings, the source model is trained on the source domain in a supervised manner, same as [15], [18], [20].

Networks. Our LCFD involves two networks: the ViL model and the target model. In practice, we choose CLIP [11] as the ViL model. The target model’s structure is the same as the source model. Following [15], [19], a target model consists of a feature extractor and a classifier (a FC layer). We adapt the feature extractor, which pre-trained on ImageNet. For fair comparison, we use ResNet101 as the backbone for VisDA and ResNet50 for the others.

Training. There are three parameters with LCFD: α in L_{EC} (Eq. (13)), σ and τ in L_{IC} (Eq. (14)). For all settings, we adopt the same configuration $(\alpha, \sigma, \tau) = (0.003, 0.4, 1.0)$. Here, since the value of \mathcal{L}_{VMI} is large, α is set to the small one of 0.003. For model training, we use the batch size of 64, SGD optimizer with momentum 0.9 and 15 epochs on all datasets. The prompt template for initialization is ‘a photo of a [CLASS].’ [11].

4.2 Closed-Set SFDA

Data sets. In this part, we evaluate LCFD on three challenging benchmarks for domain adaptation. **Office-Home** [45] is

a middle-scale dataset. It contains 15k images belonging to 65 categories from working or family environments, being divided into four domains, i.e., Artistic images, Clip Art, Product images, and Real-word images. **VisDA** [46] is a large-scale dataset. It includes 12 types of Synthetic to Real transfer recognition tasks. The source domain contains 152k synthetic images, whilst the target domain has 55k real object images from Microsoft COCO. **DomainNet-126** [47] is another large-scale dataset. As a subset of DomainNet containing 600k images of 345 classes from 6 domains of different image styles, this dataset has 145k images from 126 classes, sampled from 4 domains, Clipart, Painting, Real, Sketch, as [47] identifies severe noisy labels in the dataset.

Competitors. To evaluate LCFD, we select 14 state-of-the-art comparisons divided into three groups. (i) *The first* is the source model and CLIP that lay the basis for LCFD. (ii) *The second* is the UDA method DAPL [48], PADCLIP [49], ADCLIP [50] that introduces prompt learning to boost the cross-domain transfer. (iii) *The third* includes 9 SFDA methods: SHOT [15], GKD [25], NRC [18], SFDE [6], AdaCon [51], CoWA [23], PLUE [17], TPDS [52]. According to idea, SHOT, GKD, CoWA are pseudo-labels-based methods; NRC, PLUE, AdaCon, SFDE exploit the data geometry, e.g., the nearest neighbor, source prototype; TPDS predicts the target probability distribution using error control.

For comprehensive comparisons, we implement LCFD in two variants: (i) LCFD-C-RN (base) and (ii) LCFD-C-B32 (premium). The key distinction lies in the backbone of the CLIP image-encoder. Specifically, for LCFD-C-RN, ResNet101 is employed on the VisDA dataset, while ResNet50 is used on

TABLE 4: One step adapting results (%) on **Office-Home** in Generalized SFDA setting. S, T, H are the results on the source and target domains, and harmonic mean accuracy, respectively; the bracket values in red are the gap between S and T; WAD means With Anti-forgetting Design.

Method	Venue	WAD	S	Avg. T (S-T gap)	H
Source	-	x	98.1	59.2 (38.9)	73.1
SHOT	ICML20	x	84.2	71.8 (12.4)	77.1
GKD	IROS21	x	86.8	72.5 (14.3)	78.7
NRC	NIPS21	x	91.3	72.3 (19.0)	80.4
AdaCon	CVPR22	x	88.2	65.0 (23.2)	74.4
CoWA	ICML22	x	91.8	72.4 (19.4)	80.6
PLUE	CVPR23	x	96.3	66.9 (29.4)	78.4
TPDS	IJCV23	x	83.8	73.5 (10.3)	78.0
GDA	ICCV21	✓	80.0	70.2 (9.8)	74.4
PSAT-ViT	TMM23	✓	86.4	83.6 (2.8)	85.0
LCFD-C-RN	-	x	85.0	77.6 (7.4)	80.7
LCFD-C-B32	-	x	86.3	83.3 (3.0)	84.5

the Office-Home and DomainNet-126 datasets. On the other hand, LCFD-C-B32 adopts ViT-B/32 [53] as the backbone across all datasets. Similarly, all comparison methods using CLIP are marked with the same meaning for a convenience observation.

Comparison results. The quantitative comparisons are listed in Tab. 2~3. In the transfer task view, the group of LCFD-C-RN and LCFD-C-B32 performs best on all tasks on the three evaluation datasets. Compared with previous best SFDA methods TPDS (on Office-Home), PLUE (on VisDA) and GKD (on DomainNet-126), LCFD-C-RN improves by **4.1%**, **1.0%** and **9.3%** in average accuracy, respectively. Compared with these UDA methods with both access to labelled source data and CLIP, LCFD-C-RN still improves by **1.0%**, **0.8%** and **2.8%** on the top of second-best methods PADCLIP-RN (on Office-Home, VisDA) and ADCLIP-RN (on DomainNet-126). Also, the improvement further expanded when we switched focus to strong version LCFD-C-B32. Such results are unsurprising since the well-pre-trained CLIP is employed to identify the external causal elements.

On the other hand, LCFD-C-RN defeats CLIP-RN on all tasks, achieving the improvement of **4.5%**, **5.6%** and **5.3%** on Office-Home, VisDA and DomainNet-126 in average, respectively. Similarly, compared with CLIP-B32, the corresponding improvement of LCFD-C-B32 are changed to **7.2%**, **6.4%** and **3.7%**. This indicates the effect of the prompt learning to discover the external causal elements.

4.3 Generalized SFDA

Data sets. This setting evaluates LCFD on the Office-Home, following previous generalized SFDA methods [3], [8].

Evaluation protocol. Unlike closed-set SFDA, the generalized SFDA problem highlights the anti-forgetting ability on the seen source domain. In terms of evaluation rule, the same as [3], we adopt the harmonic mean accuracy that is computed by $H = (2 * A_s * A_t) / (A_s + A_t)$ where A_s and A_t are the accuracy on the source domain and the target domain, respectively. Note that the A_s is computed based on the source-testing set. The same to [3], [8], on the source domain, the ratio of training and testing sets is 9:1.

Competitors. As listed in Tab. 4, two generalized SFDA methods GDA [3], PSAT [8] are additionally selected as the comparisons. In GDA, domain attention was integrated with

a local clustering-based self-supervised learning method. Essentially, the capacity for the old tasks is kept by encouraging the model parameters closed to the original values. Unlike GDA, PSAT enforces the adaptation process to remember the source domain by imposing source guidance, building a target domain-centric anti-forgetting mechanism.

One step adapting comparison. Tab. 4 reports the results on Office-Home, including H-accuracy, S-accuracy and T-accuracy. In the average H-accuracy aspect, LCFD-C-B32 is only defeated by generalized SFDA method PSAT (having particular design of anti-forgetting mechanism and based on ViT backbone) with a gap of **0.5%**. Adopting the weak version LCFD-C-RN still outperforms other methods except for the best PSAT. Although T-accuracy of NRC, CoWA closes LCFD-C-RN due to the high S-accuracy (91%), the S-T gap of them (19%) is much larger than LCFD-C-RN (7.4%). These results imply a better balance of LCFD as one-step adapting.

Continual adapting results. For a comprehensive evaluation, we also conduct continual adaptation testing like [3]. For example, in the adaptation path of Ar→Cl→Pr→Rw, we first train the initial model on domain Ar. Subsequently, this trained starting model serves as the source model for adaptation to domain Cl, facilitated by LCFD. After that, the newly adapted model assumes the role of the source model for subsequent adaptation to domain Pr. In a similar way, this sequential adaptation process is iteratively executed for the final domain Rw, thus culminating in the acquisition of four distinct models. By testing the obtained four models on all domains (in each domain, **10%** data are randomly collected as the test set), we obtain the continual adaptation results, as presented in the first sub-table of Tab. 5 where the first column indicates the adaptation sequence.

Tab. 5 presents the continual adapting results of LCFD-C-RN and LCFD-C-B32. It is seen that they have a very similar pattern. Based on the LCFD-C-B32's results listed in the Bottom of Tab. 5, the observations are in two folds. **First**, if a domain is seen on the continual adapting path, the adapted model will not significantly degrade on the seen domain. For example, on the typical path of Cl→Ar→Pr→Rw, when the model adapts from Cl to Ar, the accuracy on Ar reaches **83.4%**. Compared with it, the performances of the successive adaption (to Pr and Rw) decrease by **3.7%** in average (see the second column in the second sub-table). **Second**, the adapted model also works well on the unseen domain. For example, as the adaptation goes along the path of Ar→Cl→Pr→Rw, the accuracy of the adapted model on Rw increases gradually from **71.1%** to **87.7%** (see the fifth column in the first sub-table). These results are understandable since LCFD captures the causal factors, which is robust to domain switching.

4.4 Open-Set & Partial-Set SFDA

Data sets. In this setting, we adopt Office-Home as the evaluation benchmark, as done in [9], [15].

Competitors. Besides methods Source, CLIP, SHOT, CoWA from the closed-set setting, this part adds three new comparisons HCL [54], AaD [55] and CRS [9] that all follow the contrastive learning framework.

Comparison results. As the comparison results on Office-Home presented in Tab. 6, in average accuracy, LCFD-C-B32 surpasses not only all comparisons with an improvement

TABLE 5: Continual adaptation results (%) on **Office-Home** under Generalized SFDA setting, the first column of each sub-table indicates the adaptation sequence. ↓ means the average accuracy drop of a test domain on the adaptation path compared with the performance when the domain is first seen.

ResNet50 (RN)																				
	Test					Test					Test					Test				
	Ar	Cl	Pr	Rw		Cl	Ar	Pr	Rw		Pr	Ar	Cl	Rw		Rw	Ar	Cl	Pr	
Ar	97.8	46.1	68.4	71.1	Cl	97.5	52.5	65.8	61.5	Pr	99.6	52.2	40.8	71.3	Rw	98.1	63.1	46.3	78.5	
Cl	80.0	63.5	64.3	66.0	Ar	80.1	77.8	70.7	75.6	Ar	91.2	78.4	50.2	78.3	Ar	93.4	78.4	50.4	75.6	
Pr	78.4	61.7	85.0	76.2	Pr	75.4	74.4	86.9	78.1	Cl	81.5	71.9	61.5	69.9	Cl	83.0	74.7	62.1	69.7	
Rw	83.1	60.2	83.2	84.4	Rw	67.6	78.4	85.4	85.6	Rw	87.3	76.9	59.2	85.6	Pr	87.3	72.5	61.5	85.2	
↓	17.3	2.5	1.8	—	↓	23.1	1.4	1.6	—	↓	13.0	4.1	2.3	—	↓	10.2	4.8	0.6	—	
ViT-B/32 (B32)					Test				Test				Test				Test			
	Test					Test					Test					Test				
	Ar	Cl	Pr	Rw		Cl	Ar	Pr	Rw		Pr	Ar	Cl	Rw		Rw	Ar	Cl	Pr	
Ar	97.8	46.1	68.4	71.1		97.5	52.5	65.8	61.5		99.6	52.2	40.8	71.3		98.1	63.1	46.3	78.5	
Cl	84.1	77.0	69.3	72.5		80.9	83.4	72.3	77.0		90.0	82.5	49.4	80.1		94.0	82.8	51.2	76.8	
Pr	82.5	70.9	91.0	81.1		74.2	78.1	90.4	82.2		83.6	75.6	76.2	76.2		85.2	73.8	76.2	72.5	
Rw	86.3	67.6	88.3	87.7		69.5	81.3	88.9	89.1		89.8	79.1	69.5	87.7		89.5	76.9	71.5	90.0	
↓	13.5	7.7	2.7	—		22.6	3.7	1.5	—		11.8	5.2	6.7	—		8.5	7.5	4.7	—	

TABLE 6: Partial-set SFDA and open-set SFDA results on the **Office-Home** dataset (%).

Partial-set SFDA			Open-set SFDA		
Method	Venue	Avg.	Method	Venue	Avg.
Source	—	62.8	Source	—	46.6
SHOT	ICML20	79.3	SHOT	ICML20	72.8
HCL	NIPS21	79.6	HCL	NIPS21	72.6
CoWA	ICML22	83.2	CoWA	ICML22	73.2
AaD	NIPS22	79.7	AaD	NIPS22	71.8
CRS	CVPR23	80.6	CRS	CVPR23	73.2
LCFD-C-RN	—	82.9	LCFD-C-RN	—	79.6
LCFD-C-B32	—	85.8	LCFD-C-B32	—	83.4

of **2.6%** and **10.2%** compared with previous work CoWA (partial-set) and CRS (open-set). As for LCFD-C-RN, only CoWA beat it in the partial-set setting with a tiny leading of **0.3%**. The quantitative results indicate that LCFD is still competitive on the partial-set and open-set settings.

4.5 Source-Free Out-Of-Distribution Generalization

Data sets. This part evaluates LCFD in the SF-OODG setting based on four challenging **ImageNet Variants** dataset published in recent years. Specifically, **IN-V2** (i.e., ImageNet-V2) [56] is an independent set consisting of natural images, collected from different sources, totally containing 10k images of 1000 ImageNet categories. **IN-A** (i.e., ImageNet-A) [57] is a challenging set consisting of these “natural adversarial examples” (misclassified by a vanilla ResNet50 [58]), containing 7.5k images of 200 ImageNet categories. **IN-R** (i.e., ImageNet-R) [59] is an ImageNet sub-set with artistic renditions. It contains 30k images covering 200 ImageNet categories. **IN-K** (i.e., ImageNet-Sketch) [60] collects black and white sketches from the ImageNet validation set. This dataset contains 50k images from 1000 ImageNet categories.

Competitors. As shown in Tab. 7, besides these comparison methods adopted in the closed-set SFDA setting, we add four new comparisons, CoOP [44], CoCoOp [61], TPT [26] and ProGrad [62]. Among them, CoOP, CoCoOp, ProGrad perform prompt learning under the supervision of a few labels, whilst TPT proposes self-supervised prompt tuning via minimizing the multi-view entropy. Like the closed-set setting, the CLIP-based methods are marked with the backbone of image-encoder in CLIP.

TABLE 7: SF-OODG results (%) on **ImageNet variants**. L and M means label-required and multimodal, respectively.

Method	Venue	L	M	ImageNet→X				
				IN-V2	IN-K	IN-A	IN-R	Avg.
Source	—	—	—	62.7	22.2	0.7	35.1	30.2
CLIP-RN	ICML21	—	✓	51.5	33.3	21.8	56.1	40.7
CLIP-B32	ICML21	—	✓	54.8	40.8	29.5	66.2	47.8
CoOP-RN	IJCV21	✓	✓	55.4	34.7	23.1	56.6	42.4
CoOP-B32	IJCV21	✓	✓	58.2	41.5	31.3	65.8	49.2
CoCoOp-RN	CVPR22	✓	✓	55.7	34.5	23.3	57.7	42.8
CoCoOp-B32	CVPR22	✓	✓	56.6	40.7	30.3	64.1	47.9
TPT-RN	NIPS22	✗	✓	54.7	35.1	26.7	59.1	43.9
ProGrad-RN	ICCV23	✓	✓	54.7	34.4	23.1	56.8	42.2
ProGrad-B32	ICCV23	✓	✓	57.4	41.7	31.9	66.5	49.4
SHOT	ICML20	✗	✗	62.5	38.4	2.1	42.7	36.4
GKD	IROS21	✗	✗	62.3	38.2	2.1	42.2	36.2
NRC	NIPS21	✗	✗	61.5	0.9	1.3	28.9	23.1
AdaCon	CVPR22	✗	✗	50.9	18.5	2.0	38.6	27.5
CoWA	ICML22	✗	✗	62.7	37.8	1.7	46.3	37.1
PLUE	CVPR23	✗	✗	53.0	18.5	2.0	38.6	28.0
TPDS	IJCV23	✗	✗	62.9	35.0	2.9	48.4	37.3
LCFD-C-RN	—	✗	✓	64.4	42.6	22.3	61.5	47.7
LCFD-C-B32	—	✗	✓	64.7	48.4	30.6	71.0	53.7

Comparison results. Tab. 7 reports the SF-OODG results on ImageNet Variations. In terms of average accuracy, our methods, LCFD-C-NR and LCFD-C-B32, are significantly ahead of the previous SFDA methods, improving by **10%** at least. For CLIP and the CLIP-based methods, the advantage of LCFD is still noticeable. Taking results of the weak version as an example, while improving by **7.0%** compared with CLIP-C-RN, LCFD-C-NR surpasses the second-best CLIP-based method TPT-RN by **3.8%**.

4.6 Further Discussion

During this entire discussion, all experiments are based on the strong version of LCFD, i.e., LCFD-C-B32. For brevity, we remove the suffix ‘-C-B32’.

4.6.1 Analysis for Causal Factors Discovery

This part conducts the causality analysis in two aspects. Taking the task Ar→Cl of Office-Home in closed-set setting as a toy example, we first perform a pseudo-label quality comparison to explore the discovery process. Following that, the robustness analysis to noise is carried out to evaluate the causality of the discovered causal factors, i.e., S in SFDA-specific SCM given by Fig. 1(b).

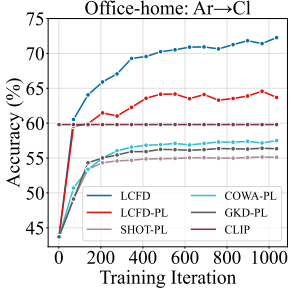


Fig. 5: Accuracy changing of pseudo-label as training iteration going on.

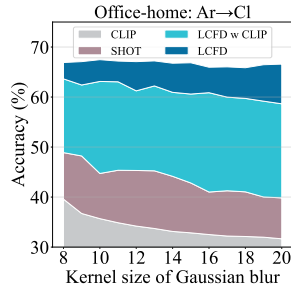


Fig. 6: Stacked area chart of accuracy as Gaussian blur intensity enhancing.

Analysis of discovering process. In our LCFD framework, the latent external causal elements S_e are captured and transformed into the observed pseudo-label. Thereby, the pseudo-label quality should be an indicator reflecting the discovery process. Here, we select the pseudo-label-based methods SHOT, COWA, GKD and CLIP’s zero shot (termed CLIP) as evaluation references. The comparison results are depicted in Fig. 5. Due to conducting S_e discovery with the aid of CLIP, the pseudo-label accuracy of LCFD, i.e., LCFD-PL, is much better than previous methods as well as CLIP-PL. On the other hand, LCFD’s curve is on the top of LCFD-PL with a significant gap during the entire training process. This phenomenon shows that capturing internal causal elements S_i is effective.

Causality evaluation of discovered causal factors. Ideally, when a model is designed to establish underlying causal relationships accurately, the model will exhibit immunity/robustness to noise [27]. To evaluate the captured causal factors, we conduct a robustness analysis to noise. Specifically, we observe the accuracy change, whilst gradually increasing the kernel size of Gaussian blur (from 8 to 20) on the input target images. The comparison methods are CLIP, SHOT and LCFD-w-CLIP, which is a variation of LCFD where the pseudo-labels adopt the zero-shot results of CLIP directly.

As shown in Fig. 6, the performance of LCFD-w-CLIP, SHOT, CLIP deteriorates to varying degrees, as noise increases. In contrast, LCFD almost maintains the performance on all intensities. Specifically, compared with the accuracy at kernel size equals 8, LCFD-w-CLIP, SHOT, CLIP respectively decrease by 5.0%, 9.1% and 7.9% when kernel size equals 20, i.e., max noise intensity, whilst the decrease of LCFD is only 0.3%. The lower performance loss of LCFD implies the effectiveness of capturing causal factors by LCFD. In particular, together LCFD with CLIP, LCFD can work with impressive noise robustness as CLIP’s zero shot performance is sharply weakening. This result implies that LCFD’s performance is not due to CLIP’s excellent zero-shot capability, but deriving from the discovery of causal factors.

Also, comparing LCFD with LCFD-w-CLIP, the gap between them gradually broadens, implying capturing the external elements S_e enables LCFD to gain immunity to noise. To gain a better understanding, we visualize the prediction distribution of LCFD-PL and CLIP at zero and max noise intensity, using the t-SNE tool. Fig. 7 displays the visualization results.

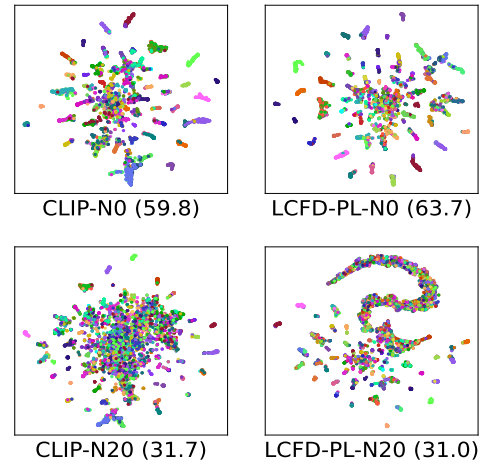


Fig. 7: Prediction visualization of LCFD-PL, CLIP when Gaussian blur kernel sizes are 0 (N0) and 20 (N20), respectively. Their corresponding classification accuracy (%) is bracketed.

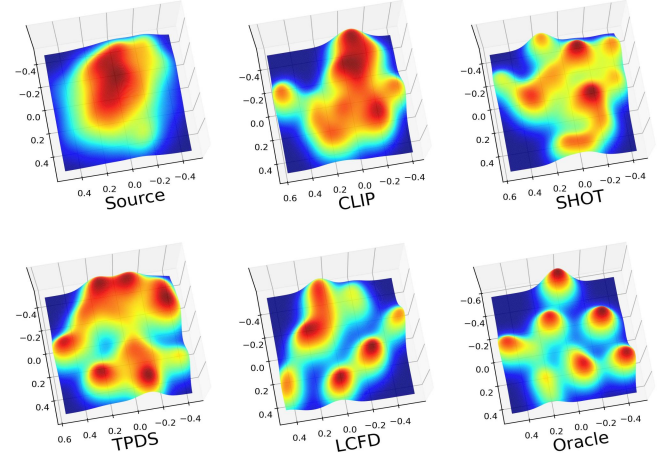


Fig. 8: Logit distribution visualization on task Ar→Cl in the **Office-Home** dataset where Oracle is trained on domain Cl by the real labels. For a clear view, the first ten categories are displayed.

When Gaussian blur kernel size is 0 (the first row), the clustering shape of LCFD-PL-N0 and CLIP-PL-N0 have a similar pattern: Samples with ambiguous semantics are mainly distributed in the middle area. As the kernel size reaches 20, CLIP-N20 continues the previous distribution pattern that ambiguous samples spread to a much wider central zone. Thereby, the noise drowns out the accurate category information provided by generated pseudo labels. As a result, the LCFD-w-CLIP’s performance deteriorates.

On the contrary, despite the accuracy being almost the same as CLIP-N20 (31%), LCFD-PL-N20 evolves a new pattern: While these ambiguous samples move to the periphery of the distribution, the remaining samples still cluster in the middle area with a shape similar to the LCFD-PL-N0 case. That is, as the noise enhancing, LCFD-PL-N20 maintains the distribution information. Correspondingly, with LCFD-PL-N20 guidance, LCFD achieves robustness to noise.

TABLE 8: Ablation study results (%). CS, OS, PS and GS mean the closed-set, open-set, partial-set and Generalised SFDA settings, respectively.

Method	Office-Home				IN-K SF-OODG	
	CS	OS	PS	GS		
Source	59.2	46.6	62.8	73.1	60.4	30.2
LCFD-w- S_i	70.3	71.5	70.1	75.9	72.6	36.9
LCFD-w- S_e	81.6	80.7	84.1	84.3	82.2	44.2
LCFD-w-CLIP	80.9	78.3	83.9	82.5	80.6	44.2
LCFD	83.3	83.4	85.8	84.5	83.7	48.4

TABLE 9: Scalability study (%) of IC instantiation.

Loss	Method	Closed-set		SF-OODG
		Office-Home	VisDA	
\mathcal{L}_{UN}	LCFD+ENT	82.5	89.4	46.8
	LCFD+NRC	83.0	87.9	47.5
	LCFD+TPDS	83.5	90.2	45.0
\mathcal{L}_{PL}	LCFD+ $\ \cdot\ _1$	82.3	88.2	44.9
	LCFD+ $\ \cdot\ _2$	82.8	88.2	40.3
	LCFD+KL	83.5	89.1	49.1
LCFD		83.3	89.2	48.4

4.6.2 Model Analysis

Feature distribution visualization. Feature distribution is an intuitive evaluation means for classification. Here, we select five comparisons, including the source model (termed Source), CLIP, SHOT, TPDS and Oracle (trained on domain Cl with the real labels). Fig. 8 shows the logit visualization results in 3D Density chart. From Source to LCFD, the clustering effect gradually strengthens, and LCFD is the most similar to Oracle.

Ablation study. In the proposed framework, we discover the causal factors $S = \{S_e, S_i\}$ in a separate way. We isolate the effect of this strategy by three variation LCFD methods. (i) LCFD-w- S_i : We only take \mathcal{L}_{UN} in Eq. (14) as the objective for model training, such that we test the effect of S_i capturing. (ii) LCFD-w- S_e : We only perform the pseudo-label supervised learning, regulated by \mathcal{L}_{PL} , where the pseudo-label is generated from S_e discovery regulated by \mathcal{L}_{EC} . Thus, the effect of S_e capturing is tested. (iii) LCFD-w-CLIP: We directly adopt the zero-shot results of CLIP as the pseudo-labels regulating the S_i discovery.

Tab. 8 reports the accuracy of these methods above in the four SFDA settings and SF-OODG. Specifically, when LCFD-w- S_i or LCFD-w- S_e works, the result outperforms Source, but significantly lower than the full version LCFD. The results indicate that individual capturing of S_e or S_i is effective, and they jointly contribute to the final performance. Also, the comparison of LCFD-w-CLIP and LCFD confirm the effect of \mathcal{L}_{EC} -based prompt learning for S_e discovery.

Scalability study of IC instantiation. The objective \mathcal{L}_{IC} in Eq. (14) regulating S_i discovery is a salable component with multiple implementations. To verify its scalability, this part respectively gives three other instantiations for the two regulators in \mathcal{L}_{IC} . For \mathcal{L}_{UN} , (i) the alone entropy regulating without category balance constraint (LCFD+ENT), (ii) data local structure-based regulating (LCFD+NRC) and (iii) domain shift control-based regulating (LCFD+TPDS) are selected as alternatives. For \mathcal{L}_{PL} , the popular 1-Norm ($\|\cdot\|_1$), 2-Norm ($\|\cdot\|_2$) and KL divergence are employed.

As the results listed in Tab. 9, in the closed-set setting,

TABLE 10: Prompt initialization study (%).

# Initialization template	Closed-set		SF-OODG
	Office-Home	VisDA	
1 'X [CLASS].' (#X=4)	82.6	89.1	48.4
2 'X [CLASS].' (#X=16)	81.5	88.5	46.1
3 'There is a [CLASS].'	83.6	89.2	48.6
4 'This is a photo of a [CLS].'	83.7	89.0	48.8
5 'This is maybe a photo of a [CLS].'	83.0	89.1	48.8
6 'This is almost a photo of a [CLS].'	83.7	89.2	48.4
7 'This is definitely a photo of a [CLS].'	83.5	88.9	48.1
8 'a picture of a [CLS].'	83.5	88.8	48.6
9 'a photo of a [CLS].'	83.3	89.2	48.4

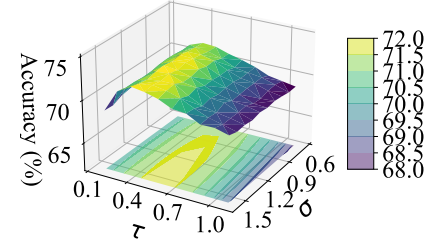


Fig. 9: Parameter sensitiveness study (σ, τ) on task Ar→Cl in Office-Home.

LCFD+TPDS obtain the best results, and other methods have a gap of up to 2%. This indicates that these typical regulators do not substantially impact model performance in the closed-set setting. In the SF-OODG setting, besides LCFD+KL, all methods have a certain accuracy decrease compared with LCFD. For LCFD+ENT, removing category balance regulating leads to a decrease. The decrease of LCFD+NRC and LCFD+TPDS is due to the method not specifically considering the SF-OODG setting. Regarding the \mathcal{L}_{PL} group, the results indicate that probability distribution approximation (KL) outshines the features closing ($\|\cdot\|_1, \|\cdot\|_2$) in terms of maintaining the model performance caused by the external causal elements.

Effect of prompt initialization. In the LCFD method, we adopt prompt learning to encode the external causal factors S_e . In this part, we give four kinds of initialization strategies to figure out the effect of prompt initiation. As listed in Tab. 10, except for conventional (i) constant strategy (row 1~2), (ii) sentence strategy (row 3~4) and (iii) phrase strategy (row 5~7), we introduce an interesting strategy of sentence initialization with uncertainty (row 8~9), considering the lacking of accurate supervision in SFDA.

Tab. 10 gives the comparison results of nine templates in the closed-set setting and SF-OODG. It can be observed that these templates do not lead to significant performance variance. These results indicate that the LCFD model is insensitive to prompt selection. Meanwhile, comparing the constant strategy and other strategies, the initialization with semantics is a better option, which also meets our expectations.

Parameters sensitiveness. Taking the task Ar→Cl in Office-Home as a toy experiment, we present the LCFD performance varying as hyper-parameters $0.2 \leq \sigma \leq 1.1$, $0.7 \leq \tau \leq 1.6$ with 0.1 steps. As depicted in Fig. 9, the

accuracy-varying surface does not have evident vibrations. This observation suggests that LCFD is insensitive to alterations in σ and τ .

5 CONCLUSION

This paper considers a more challenging Unified SFDA problem that thoroughly addresses all specific scenarios in a unified manner. Further, we propose a LCFD approach from a causality view, conceptually different from prior statistical dependence-based scheme. Specifically, we propose a self-supervised information bottleneck to capture the external ones and further transform them into pseudo-labels to regulate the successive IC process for discovering internal ones. According to our theoretical result, we instantiate the proposed information bottleneck based on the network implementation for variational mutual information. Extensive experiments on four mainstream SFDA settings and SF-OODG validate the superiority of our LCFD.

Acknowledgments

This work is partially supported by the German Research Foundation and National Natural Science Foundation of China (NSFC) in project Crossmodal Learning under contract Sonderforschungsbereich Transregio 169, the Hamburg Landesforschungsförderungsprojekt Cross, NSFC (61773083); Horizon2020 RISE project STEP2DYNA (691154); NSFC (62206168, 62276048).

REFERENCES

- [1] Y. Kim, D. Cho, K. Han, P. Panda, and S. Hong, "Domain adaptation without source data," *IEEE Trans. on Artif. Intell.*, vol. 2, no. 6, pp. 508–518, 2021.
- [2] R. Li, Q. Jiao, W. Cao, H.-S. Wong, and S. Wu, "Model adaptation: Unsupervised domain adaptation without source data," in *Proc. IEEE Conf. Comput. Vis. Pattern Recog. (CVPR)*, 2020, pp. 9641–9650.
- [3] S. Yang, Y. Wang, J. Van De Weijer, L. Herranz, and S. Jui, "Generalized source-free domain adaptation," in *Proc. IEEE Int. Conf. Comput. Vis. (ICCV)*, 2021, pp. 8978–8987.
- [4] P. Panareda Busto and J. Gall, "Open set domain adaptation," in *Proc. IEEE Int. Conf. Comput. Vis. (ICCV)*, 2017, pp. 754–763.
- [5] Z. Cao, K. You, M. Long, J. Wang, and Q. Yang, "Learning to transfer examples for partial domain adaptation," in *Proc. IEEE Conf. Comput. Vis. Pattern Recog. (CVPR)*, 2019, pp. 2985–2994.
- [6] N. Ding, Y. Xu, Y. Tang, C. Xu, Y. Wang, and D. Tao, "Source-free domain adaptation via distribution estimation," in *Proc. IEEE Conf. Comput. Vis. Pattern Recog. (CVPR)*, 2022, pp. 7212–7222.
- [7] Y. Luo, Z. Wang, Z. Chen, Z. Huang, and M. Bakhtashmotlagh, "Source-free progressive graph learning for open-set domain adaptation," *IEEE Trans. Pattern Anal. Mach. Intell.*, 2023.
- [8] S. Tang, Y. Shi, Z. Song, M. Ye, C. Zhang, and J. Zhang, "Progressive source-aware transformer for generalized source-free domain adaptation," *IEEE Trans. on Multimedia*, 2023, dOI: <https://doi.org/10.1109/TMM.2023.3321421>.
- [9] Y. Zhang, Z. Wang, and W. He, "Class relationship embedded learning for source-free unsupervised domain adaptation," in *Proc. IEEE Conf. Comput. Vis. Pattern Recog. (CVPR)*, 2023, pp. 7619–7629.
- [10] J. Pearl, *Causality*. Cambridge university press, 2009.
- [11] A. Radford, J. W. Kim, C. Hallacy, A. Ramesh, G. Goh, S. Agarwal, G. Sastry, A. Askell, P. Mishkin, J. Clark, et al., "Learning transferable visual models from natural language supervision," in *Proceedings of the Int. Conf. Mach. Learn. (ICML)*. PMLR, 2021, pp. 8748–8763.
- [12] R. Li, Q. Jiao, W. Cao, H. Wong, and S. Wu, "Model adaptation: Unsupervised domain adaptation without source data," in *Proc. IEEE Conf. Comput. Vis. Pattern Recog. (CVPR)*, 2020, pp. 9638–9647.
- [13] J. Tian, J. Zhang, W. Li, and D. Xu, "VDM-DA: Virtual domain modeling for source data-free domain adaptation," *IEEE Trans. Circuits Syst. Video Technol.*, vol. 32, no. 6, pp. 3749–3760, 2021.
- [14] Y. Du, H. Yang, M. Chen, J. Jiang, H. Luo, and C. Wang, "Generation, augmentation, and alignment: A pseudo-source domain based method for source-free domain adaptation," *arXiv:2109.04015*, 2021.
- [15] J. Liang, D. Hu, and J. Feng, "Do we really need to access the source data? source hypothesis transfer for unsupervised domain adaptation," in *Proceedings of the Int. Conf. Mach. Learn. (ICML)*, 2020, pp. 6028–6039.
- [16] W. Chen, L. Lin, S. Yang, D. Xie, S. Pu, and Y. Zhuang, "Self-supervised noisy label learning for source-free unsupervised domain adaptation," in *Proc. IEEE Int. Intell. Rob. Syst. (IROS)*. IEEE, 2022, pp. 10 185–10 192.
- [17] M. Litrico, A. Del Bue, and P. Morerio, "Guiding pseudo-labels with uncertainty estimation for test-time adaptation," in *Proc. IEEE Conf. Comput. Vis. Pattern Recog. (CVPR)*, 2023.
- [18] S. Yang, J. van de Weijer, L. Herranz, S. Jui, et al., "Exploiting the intrinsic neighborhood structure for source-free domain adaptation," *Proc. Adv. Neural Inform. Process. Syst. (NeurIPS)*, vol. 34, pp. 29 393–29 405, 2021.
- [19] S. Yang, Y. Wang, J. van de Weijer, L. Herranz, S. Jui, and J. Yang, "Trust your good friends: Source-free domain adaptation by reciprocal neighborhood clustering," *IEEE Trans. Pattern Anal. Mach. Intell.*, 2023.
- [20] S. Tang, Y. Zou, Z. Song, J. Lyu, L. Chen, M. Ye, S. Zhong, and J. Zhang, "Semantic consistency learning on manifold for source data-free unsupervised domain adaptation," *Neural Networks*, vol. 152, pp. 467–478, 2022.
- [21] W. Li and S. Chen, "Partial domain adaptation without domain alignment," *IEEE Transactions on Pattern Analysis and Machine Intelligence*, 2022.
- [22] G. Vray, D. Tomar, B. Bozorgtabar, and J.-P. Thiran, "Distill-soda: Distilling self-supervised vision transformer for source-free open-set domain adaptation in computational pathology," *IEEE Transactions on Medical Imaging*, 2024.
- [23] J. Lee, D. Jung, J. Yim, and S. Yoon, "Confidence score for source-free unsupervised domain adaptation," in *Int. Conf. Mach. Learn. (ICML)*. PMLR, 2022, pp. 12 365–12 377.
- [24] J. H. A. Samadhi, H. Gani, N. H. Hussein, M. U. Khattak, M. Naseer, F. Khan, and S. Khan, "Align your prompts: Test-time prompting with distribution alignment for zero-shot generalization," in *Thirty-seventh Conference on Neural Information Processing Systems*, 2023.
- [25] S. Tang, Y. Shi, Z. Ma, J. Li, J. Lyu, Q. Li, and J. Zhang, "Model adaptation through hypothesis transfer with gradual knowledge distillation," in *Proc. IEEE/RSJ Int. Conf. Intell. Rob. Syst. (IROS)*. IEEE, 2021, pp. 5679–5685.
- [26] M. Shu, W. Nie, D.-A. Huang, Z. Yu, T. Goldstein, A. Anandkumar, and C. Xiao, "Test-time prompt tuning for zero-shot generalization in vision-language models," *Proc. Adv. Neural Inform. Process. Syst. (NeurIPS)*, vol. 35, pp. 14 274–14 289, 2022.
- [27] B. Schölkopf, F. Locatello, S. Bauer, N. R. Ke, N. Kalchbrenner, A. Goyal, and Y. Bengio, "Toward causal representation learning," *Proceedings of the IEEE*, vol. 109, no. 5, pp. 612–634, 2021.
- [28] Y. Chen and P. Bühlmann, "Domain adaptation under structural causal models," *J. Mach. Learn. Resear. (JMLR)*, vol. 22, no. 1, pp. 11 856–11 935, 2021.
- [29] R. Christiansen, N. Pfister, M. E. Jakobsen, N. Gnecco, and J. Peters, "A causal framework for distribution generalization," *IEEE Trans. Pattern Anal. Mach. Intell.*, vol. 44, no. 10, pp. 6614–6630, 2021.
- [30] W. Wang, X. Lin, F. Feng, X. He, M. Lin, and T.-S. Chua, "Causal representation learning for out-of-distribution recommendation," in *Proc. ACM Web Conf. (WWW)*, 2022, pp. 3562–3571.
- [31] C. Ouyang, C. Chen, S. Li, Z. Li, C. Qin, W. Bai, and D. Rueckert, "Causality-inspired single-source domain generalization for medical image segmentation," *IEEE Trans. Med. Imag. (TMI)*, vol. 42, no. 4, pp. 1095–1106, 2022.
- [32] F. Lv, J. Liang, S. Li, B. Zang, C. H. Liu, Z. Wang, and D. Liu, "Causality inspired representation learning for domain generalization," in *Proc. IEEE Conf. Comput. Vis. Pattern Recog. (CVPR)*, 2022, pp. 8046–8056.
- [33] Z. Yue, Q. Sun, X.-S. Hua, and H. Zhang, "Transporting causal mechanisms for unsupervised domain adaptation," in *Proc. IEEE Int. Conf. Comput. Vis. (ICCV)*, 2021, pp. 8599–8608.
- [34] R. Wang, M. Yi, Z. Chen, and S. Zhu, "Out-of-distribution generalization with causal invariant transformations," in *Proc. IEEE Conf. Comput. Vis. Pattern Recog. (CVPR)*, 2022, pp. 375–385.
- [35] D. Mahajan, S. Tople, and A. Sharma, "Domain generalization using causal matching," in *Int. Conf. Mach. Learn. (ICML)*. PMLR, 2021, pp. 7313–7324.

[36] J. Peters, D. Janzing, and B. Schölkopf, *Elements of causal inference: foundations and learning algorithms*. The MIT Press, 2017.

[37] K. Kawaguchi, Z. Deng, X. Ji, and J. Huang, "How does information bottleneck help deep learning?" in *Proc. Int. Conf. Mach. Learn. (ICML)*. PMLR, 2023, p. 16049–16096.

[38] N. Tishby, F. C. Pereira, and W. Bialek, "The information bottleneck method," *arXiv preprint physics/0004057*, 2000.

[39] R. Houthooft, X. Chen, Y. Duan, J. Schulman, F. De Turck, and P. Abbeel, "Vime: Variational information maximizing exploration," *Proc. Adv. Neural Inform. Process. Syst. (NeurIPS)*, vol. 29, 2016.

[40] D. Barber and F. Agakov, "The im algorithm: a variational approach to information maximization," *Proc. Adv. Neural Inform. Process. Syst. (NeurIPS)*, vol. 16, no. 320, p. 201, 2004.

[41] X. Ji, J. F. Henriques, and A. Vedaldi, "Invariant information clustering for unsupervised image classification and segmentation" in *Proc. IEEE Int. Conf. Comput. Vis. (ICCV)*, 2019, pp. 9865–9874.

[42] B. Li, Y. Shen, Y. Wang, W. Zhu, D. Li, K. Keutzer, and H. Zhao, "Invariant information bottleneck for domain generalization," in *Proc. AAAI Conf. Artif. Intell. (AAAI)*, vol. 36, no. 7, 2022, pp. 7399–7407.

[43] K. Ghasedi Dizaji, A. Herandi, C. Deng, W. Cai, and H. Huang, "Deep clustering via joint convolutional autoencoder embedding and relative entropy minimization," in *Proc. IEEE Conf. Int. Conf. Comput. Vis. (ICCV)*, 2017, pp. 5736–5745.

[44] K. Zhou, J. Yang, C. C. Loy, and Z. Liu, "Learning to prompt for vision-language models," *Int. J. Comput. Vis.*, vol. 130, no. 9, pp. 2337–2348, 2022.

[45] H. Venkateswara, J. Eusebio, S. Chakraborty, and S. Panchanathan, "Deep hashing network for unsupervised domain adaptation," in *Proc. IEEE Conf. Comput. Vis. Pattern Recog. (CVPR)*, 2017, pp. 5385–5394.

[46] X. Peng, B. Usman, N. Kaushik, J. Hoffman, D. Wang, and K. Saenko, "Visda: The visual domain adaptation challenge," *arXiv:1710.06924*, 2017.

[47] X. Peng, Q. Bai, X. Xia, Z. Huang, K. Saenko, and B. Wang, "Moment matching for multi-source domain adaptation," in *Proc. IEEE Int. Conf. Comput. Vis. (ICCV)*, 2019, pp. 1406–1415.

[48] C. Ge, R. Huang, M. Xie, Z. Lai, S. Song, S. Li, and G. Huang, "Domain adaptation via prompt learning," *IEEE Transactions on Neural Networks and Learning Systems*, 2023.

[49] Z. Lai, N. Vesdapunt, N. Zhou, J. Wu, C. P. Huynh, X. Li, K. K. Fu, and C.-N. Chuah, "PADCLIP: Pseudo-labeling with adaptive debiasing in clip for unsupervised domain adaptation," in *Proc. IEEE Int. Conf. Comput. Vis. (ICCV)*, 2023, pp. 16155–16165.

[50] M. Singha, H. Pal, A. Jha, and B. Banerjee, "Ad-clip: Adapting domains in prompt space using clip," in *Proc. IEEE Int. Conf. Comput. Vis. (ICCV)*, 2023, pp. 4355–4364.

[51] D. Chen, D. Wang, T. Darrell, and S. Ebrahimi, "Contrastive test-time adaptation," in *Proc. IEEE Conf. Comput. Vis. Pattern Recog. (CVPR)*, 2022, pp. 295–305.

[52] S. Tang, A. Chang, F. Zhang, X. Zhu, M. Ye, and Z. Changshui, "Source-free domain adaptation via target prediction distribution searching," *Int. J. Comput. Vis.*, 2023, dOI: <https://doi.org/10.1007/s11263-023-01892-w>.

[53] K. Han, Y. Wang, H. Chen, X. Chen, J. Guo, Z. Liu, Y. Tang, A. Xiao, C. Xu, Y. Xu, *et al.*, "A survey on vision transformer," *IEEE Trans. Pattern Anal. Mach. Intell.*, vol. 45, no. 1, pp. 87–110, 2022.

[54] J. Huang, D. Guan, A. Xiao, and S. Lu, "Model adaptation: Historical contrastive learning for unsupervised domain adaptation without source data," *Proc. Adv. Neural Inform. Process. Syst. (NeurIPS)*, vol. 34, pp. 3635–3649, 2021.

[55] S. Yang, S. Jui, J. van de Weijer, *et al.*, "Attracting and dispersing: A simple approach for source-free domain adaptation," *Proc. Adv. Neural Inform. Process. Syst. (NeurIPS)*, vol. 35, pp. 5802–5815, 2022.

[56] B. Recht, R. Roelofs, L. Schmidt, and V. Shankar, "Do imagenet classifiers generalize to imagenet?" in *Int. Conf. Mach. Learn. (ICML)*. PMLR, 2019, pp. 5389–5400.

[57] D. Hendrycks, K. Zhao, S. Basart, J. Steinhardt, and D. Song, "Natural adversarial examples," in *Proc. IEEE Conf. Comput. Vis. Pattern Recog. (CVPR)*, 2021, pp. 15262–15271.

[58] K. He, X. Zhang, S. Ren, and J. Sun, "Deep residual learning for image recognition," in *Proc. IEEE Conf. Comput. Vis. Pattern Recog. (CVPR)*, 2016, pp. 770–778.

[59] D. Hendrycks, S. Basart, N. Mu, S. Kadavath, F. Wang, E. Dorundo, R. Desai, T. Zhu, S. Parajuli, M. Guo, *et al.*, "The many faces of robustness: A critical analysis of out-of-distribution generalization," in *Proc. IEEE Int. Conf. Comput. Vis. (ICCV)*, 2021, pp. 8340–8349.

[60] H. Wang, S. Ge, Z. Lipton, and E. P. Xing, "Learning robust global representations by penalizing local predictive power," *Proc. Adv. Neural Inform. Process. Syst. (NeurIPS)*, vol. 32, 2019.

[61] K. Zhou, J. Yang, C. C. Loy, and Z. Liu, "Conditional prompt learning for vision-language models," in *Proc. IEEE Conf. Comput. Vis. Pattern Recog. (CVPR)*, 2022, pp. 16816–16825.

[62] B. Zhu, Y. Niu, Y. Han, Y. Wu, and H. Zhang, "Prompt-aligned gradient for prompt tuning," in *Proc. IEEE Int. Conf. Comput. Vis. (ICCV)*, 2023, pp. 15659–15669.